Catalysis Today 273 (2016) 252–258

Contents lists available at ScienceDirect

Catalysis Today

journal homepage: www.elsevier.com/locate/cattod

Flexible NiZr-based structured catalysts for ethylene production through ODH of ethane: Catalytic performance enhancement

J.P. Bortolozzi, E.D. Banús, N.L. Courtalón, M.A. Ulla, V.G. Milt, E.E. Miró*

Instituto de Investigaciones en Catálisis y Petroquímica—INCAPE (FIQ, UNL-CONICET), Santiago del Estero 2829, S3000AOM Santa Fe, Argentina

ARTICLE INFO

Article history:
Received 25 November 2015
Received in revised form 5 February 2016
Accepted 1 March 2016
Available online 25 March 2016

Keywords:
Oxidative dehydrogenation of ethane
Ni catalysts
Zr promoter
Catalytic ceramic paper
Ethylene production

ABSTRACT

Flexible structured catalysts based on Ni and Zr deposited on a ceramic paper made of SiO_2-Al_2O_3 and ZrO_2 fibers showed to be active and selective for the Oxidative Dehydrogenation of Ethane. Zirconium promoter strongly interacted with nickel oxide and produced structural changes that affected the NiO redox behavior, crystal growth and lattice order which enhanced selectivity towards ethylene. The variation of the concentration of the precursor solution used and the addition of zirconia short fibers, affected the catalytic performance. The lower the concentration of the solution used to incorporate the catalyst, the better the catalytic performance. The addition of zirconia fibers also showed beneficial effects on ethylene production.

1. Introduction

Light olefins such as ethylene, propylene and butylenes are strategic products for the current chemical industry. In 2004, the total consumption of this group represented around 174 millions of tons; it rose up to 205 millions in 2010 and it is expected to grow up to 259 million tons in 2016 [1]. In particular, ethylene is a key building block to produce polyethylene, ethylene oxide, ethylene dichloride, ethyl benzene, propionaldehyde and *n*-propyl alcohol, among others. Nowadays, it is mainly produced by steam cracking of light fractions of naphtha and some components of natural gas that operates under severe conditions with temperatures above 800 °C.

Some alternative processes for the production of this key light olefin are under study, but the oxidative dehydrogenation of ethane (ODH) seems to be particularly promising. The main advantage of this method is the absence of thermodynamic constraints that enable the system to operate in mild conditions at temperatures between 300 °C and 500 °C.

Furthermore, the discovery of large reserves of shale gas has notably increased the availability of natural gas that is mainly composed of methane, but that could also contain up to 11% of ethane. This resulted in a decrease in gas costs of about 75%, relative to 2005 prices, making shale gas very attractive both as an energy source and as feedstock for the production of fuels or chemicals [1].

Over the last years, several catalysts have been studied to convert ethane into ethylene through oxydehydrogenation reaction. Among them, an important group of these catalysts is based on nickel oxide [2–4]. Although this oxide shows a higher level of activity based on its capacity to activate ethane, its selectivity to the olefin is too low. The latter can be increased by dispersing nickel species on a suitable support as SiO_2 [2], Al_2O_3 [2,5,6], MgO [7] or ZrO_2 [8]. Also, both conversion and selectivity can be modified, tuning the properties of nickel oxide by doping it with other elements like Mo, W, Nb, Ce, Sn or Ta [9–13].

A number of reports investigate these catalysts in powder form, which entail some practical constraints to any potential industrial application. In this respect, different groups have put in a great deal of effort to research on the feasibility of depositing catalytic formulations onto different substrates so as to make use of the intrinsic advantages of each type of structures. Among them, metallic and ceramic foams [14–17] and ceramic paper [18,19] were studied. Besides, some authors reported the use of metallic or ceramic monoliths [20], while others investigated the conformation of microchannel metallic reactors [21].

Based on a variety of reasons and according to each case in particular, structured catalysts can offer improved catalytic performances when compared with the corresponding powder catalysts [16]. However, in a couple of reports [14,20] it has been found that ethylene yield diminishes after the catalyst deposition onto a sub-

* Corresponding author.
E-mail addresses: emiro@fiq.unl.edu.ar, cabemiro@hotmail.com (E.E. Miró).

http://dx.doi.org/10.1016/j.cattod.2016.03.005
0920-5861/

strate. In addition, the easiness to scaling-up this kind of systems by replication should be considered as an additional advantage.

In this work we study the ethane ODH using structured catalysts containing NiO as the active compound and Zr as the promoter, both supported on ceramic paper substrates made of SiO_2-Al_2O_3 and ZrO_2 fibers. In a previous work [19], we showed that the addition of Zr as promoter produced lower ethane conversion than NiO alone, but higher selectivity to ethylene.

With the aim of improving catalytic performance, this contribution focuses on the development of catalytic ceramic paper by partially replacing SiO_2-Al_2O_3 fibers by ZrO_2 ones in order to incorporate the promoting element into the structured substrate. Moreover, the amount of catalyst incorporated was varied so as to improve ethylene yield.

2. Materials and methods

2.1. Ceramic paper preparation

Three types of fibers were used in the preparation of ceramic papers. The first one was composed of long ceramic fibers (50 wt% SiO_2, 48 wt% Al_2O_3 and 2 wt% impurities, mainly titanium and iron oxides), 660 μm length, obtained by elutriation from *Carbo Ceramic* materials. The elutriation process was performed with the aim of both homogenize the size of the fibers and to eliminate the soluble impurities. After that, an Energy dispersive X-ray analysis (EDX) detected iron and titanium as impurities in a level lower than 1 wt% [19]. These elements are common impurities when aluminum is present. In addition, both short ZrO_2 ceramic fibers, 190 μm length, provided by *Zircar* and cellulosic ones, obtained by repulping an industrial blotting paper from bleached Kraft softwood were also employed.

A papermaking technique with a dual polyelectrolyte retention system was adopted, which implied the use of cationic and anionic polymers (Fig. 1). These polyelectrolytes generate a double layer of charged polymers on ceramic fibers and also produce bridges which join these fibers, thus increasing the retention of particles during the papermaking process. The cationic polymer was polyvinyl amine from BASF (PVAm LUREDUR PR 8095 molecular weight 4×105 g/mol and charge density 4.5 meq/g). The anionic polymer was polyacrylamide (A-PAM from AQUATEC, molecular weight 10^4–10^5 g/mol and charge density 2.7 meq/g). Commercial colloidal suspension of yttria-stabilized zirconia (Nyacol®, 18.0 wt% ZrO_2 + 1.3 wt% Y_2O_3, particle size 100 nm) was added as binder to provide mechanical strength to the final structure. This procedure is similar to that employed by Tuler et al. [22].

Two different types of flexible ceramic paper were prepared, one of them using only SiO_2-Al_2O_3 fibers and the other replacing 10 wt% SiO_2-Al_2O_3 fibers by the same amount of ZrO_2 fibers.

After calcination at 600 °C during 2 h in air cellulosic fibers were burnt and ceramic paper was obtained, designating LF the paper that only contains SiO_2-Al_2O_3 fibers and SF the one that also contains short ZrO_2 fibers.

2.2. Catalytic components incorporation

In order to develop catalytic ceramic paper, ceramic paper sheets (16 cm in diameter, prepared as described in Section 2.1) were cut into disc forms (16 mm in diameter and 2 mm in thickness). Single or mixed solutions were used to prepare Ni and NiZr ceramic paper. Both 0.3 and 0.4 M $Ni(NO_3)_2$ solutions were used and in the case of Zr-containing paper, a 0.2 M $Zr(NO_3)_4$ solution was also incorporated as promoter. Ceramic paper discs were moistened up to saturation with the above mentioned solutions and citric acid (CA) acting as coordination ligand was also added. Two

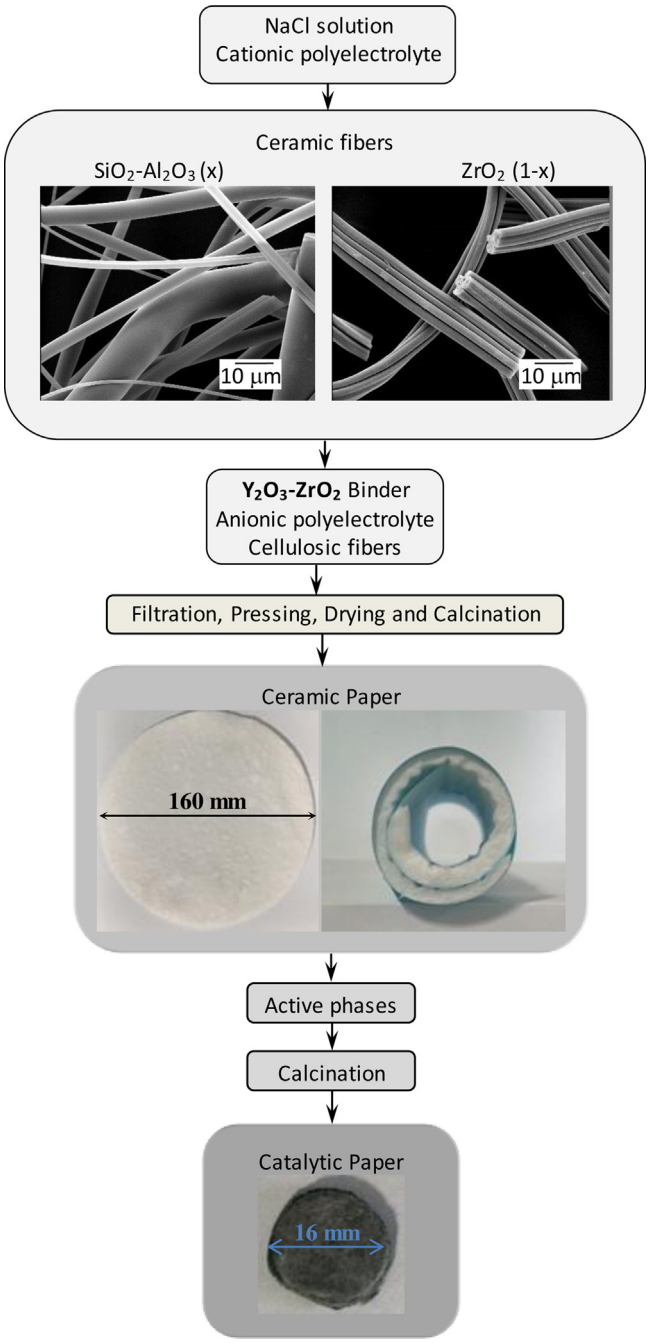

Fig. 1. Synthesis procedure of the catalytic ceramic paper. Detail of the ceramic fibers.

Zr/Ni atomic ratios of 0.11 or 0.15, which were almost the optimal, were studied [23]. After drying at room temperature for 24 h, the impregnated paper was calcined in air at 500 °C during 2 h.

The structured catalysts thus obtained were designated according to the active phases (Ni or NiZr) incorporated, the precursor solution concentrations (0.3 or 0.4 M) used and the type of fiber used in the papermaking process, SiO_2-Al_2O_3 fibers (LF) or 10 wt% ZrO_2 fibers + 90 wt% SiO_2-Al_2O_3 fibers (SF).

2.3. Physicochemical characterization

X-ray Diffraction (XRD): Crystalline phases were identified with Shimadzu XD-D1 equipment using Cu Kα radiation at a scan rate of 2°/min, from $2\theta = 20°$ to 80°. The ceramic paper pieces were

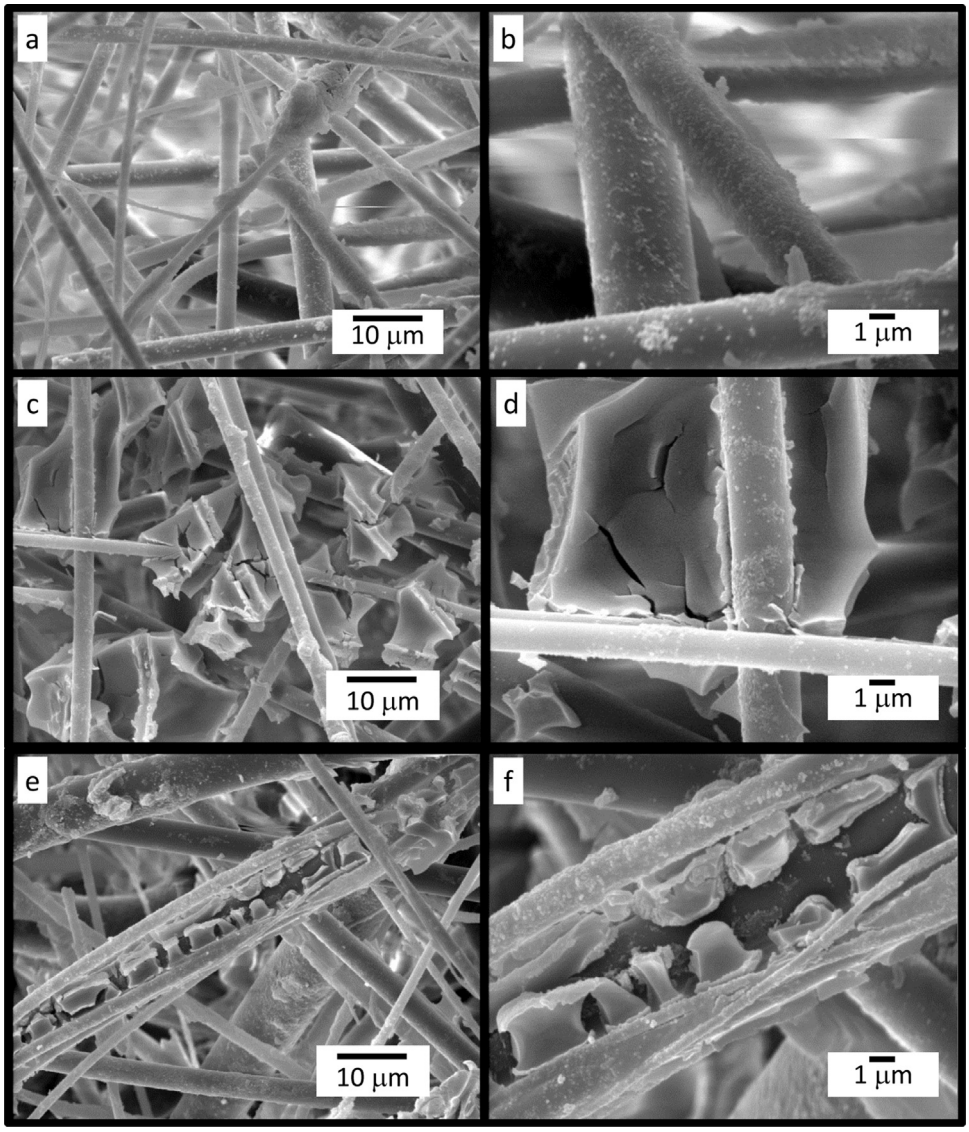

Fig. 2. SEM micrographs of ceramic paper LF (a, b) and catalytic paper: NiZr 0.15 (0.3 M) LF (c, d) and NiZr 0.15 (0.4 M) LF (e, f).

supported on a special sample holder designed for the XRD analysis. The software package of the instrument was used for phase identification from the X-ray diffractograms. Crystallite sizes were estimated by the Scherrer equation, employing the main peaks (2θ) of each compound.

Laser Raman Spectroscopy (LRS): a Horiba Jobin Yvon LabRAM HR instrument was employed to obtain the spectra. The excitation wavelength was 532.13 nm (Spectra Physics diode pump solid state laser with the power set at 30 mW). Several spectra were acquired for each sample.

Scanning Electron Microscopy (SEM): an electronic microscope JEOL JSM-35C with an acceleration voltage of 20 kV was employed. Samples were coated with a thin layer of Au in order to improve image quality.

Temperature-programmed Reduction (TPR): The experiments were performed in a Micromeritics Autochem II instrument using a mixture of H_2/Ar (5%) as reducing gas. The heating rate was 10 °C/min from room temperature to 800 °C.

2.4. Catalytic tests

The oxidative dehydrogenation of ethane was performed in a temperature range between 250 and 450 °C employing a flow system. The reactive stream was 6% O_2 and 6% C_2H_6 with helium as balance gas. The adequate number of catalytic paper discs was stacked inside a quartz reactor (400 mm in length and 16 mm in diameter). Temperature measurement was performed with an axially located thermocouple. The total mass of catalyst deposited onto the paper was 200 mg (NiO or NiO + ZrO_2).

Two series of ODH experiments were performed. Firstly, the evaluation of the ethane conversion was conducted at variable temperature with a W/F fixed ratio. The standard W/F value used to compare the activity of the different catalysts was 0.48 g s/cm^3, where W corresponds to the above mentioned weight of the catalyst deposited onto the paper fibers being F the total flow rate.

In a second stage, with the aim of exploring the selectivity-conversion behavior at a fixed temperature (400 °C), the W/F ratio was modified from 0.1 to 0.8 g s/cm^3 by varying the total flow inlet (reagents + balance gas) maintaining the amount of catalyst constant.

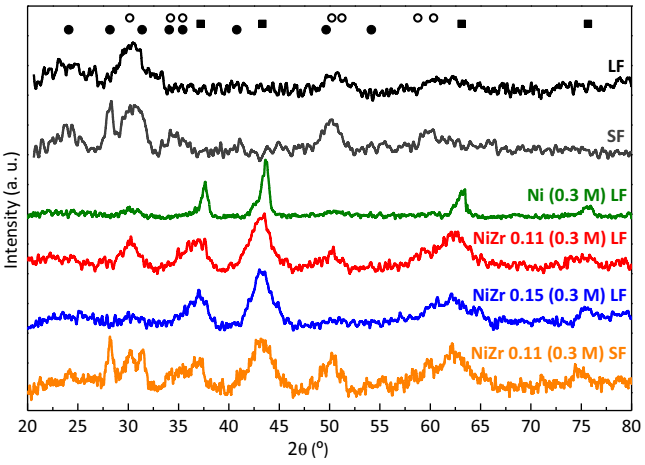

Fig. 3. XRD diffraction patterns of catalytic ceramic paper (0.3 M). Symbols: ● monoclinic ZrO_2, ○ tetragonal ZrO_2, ■ NiO.

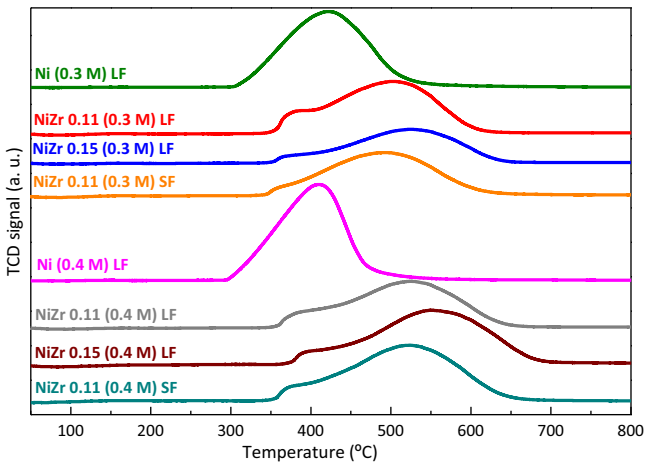

Fig. 4. Temperature-programmed reduction profiles of different kinds of catalytic paper (0.3 and 0.4 M).

Reactants and products were analyzed with an on-line Shimadzu® GC 2014 gas chromatograph equipped with a packed column (HayeSep D®) and a thermal conductivity detector (TCD). Closure of the carbon mass balance was 100 ± 3%. Carbon monoxide or other by-products were not detected in the product stream after the reaction. The total oxygen conversion never reached 100%. The downstream gas composition was measured after 1 h, to ensure that the reaction steady state was achieved. In addition, under the experimental conditions used in the catalytic tests the contribution of gas-phase reactions was negligible.

Each reaction experiment was performed at least three times for the different set of catalysts. The conversion and selectivity obtained were almost the same in all cases, considering an experimental error below 5%, which guarantees the reproducibility of the catalytic results.

3. Results and discussion

3.1. Characterization of the flexible ceramic and catalytic paper

Fig. 2a and b show the morphology of the ceramic papers containing only the Y_2O_3-stabilized ZrO_2 binder, i.e. after calcination and previous to the impregnation of active phases. The surface of the ceramic fibers appears to be completely covered with binder agent particles. Yttria-stabilized zirconia creates a homogeneous and well-dispersed coating. Besides, some clusters of the binder can be clearly observed in the intersection of two fibers. These accumulations permit the cross-linking of the fibers, thus, giving mechanical resistance to the ceramic structure (Fig. 2a). It is necessary to remember that the original fibers (before ceramic paper synthesis) present a noticeable smooth surface without pores, roughness or imperfections (Fig. 1).

Fig. 2c–f show the morphology of the catalytic ceramic paper, NiZr 0.15 (0.3 M) LF (Fig. 2c and d) and NiZr 0.15 (0.4 M) LF (Fig. 2e and f). Catalytic paper prepared using either the 0.3 M or the 0.4 M $Ni(NO_3)_2$ solutions show a similar morphology. The catalyst is homogeneously deposited between and onto ceramic fiber where the solution is retained by surface tension. After drying and calcining catalytic ceramic paper, numerous flakes and cracks are observed with ceramic fibers crossing them. Closer views (Fig. 2d and f) reveal that these flakes are ca. 1–10 μm wide and ca. 1 μm thick. SEM micrographs of the other catalytic ceramic paper are not shown because they display similar pictures.

XRD patterns of the catalytic paper prepared with the 0.3 M precursor solution are shown in Fig. 3, where those diffractograms

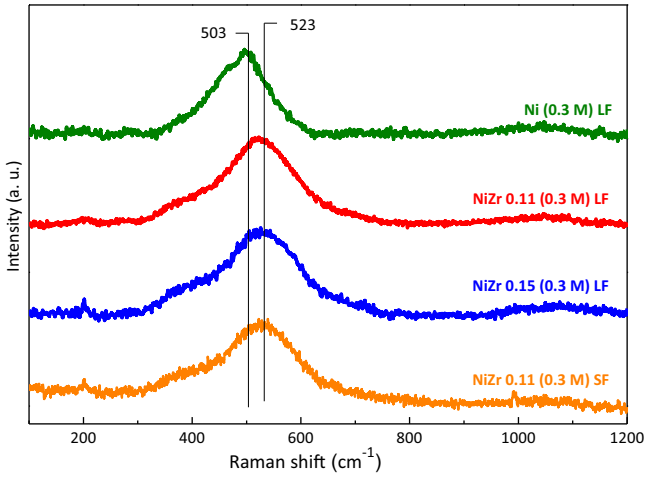

Fig. 5. Raman spectra of catalytic paper (0.3 M).

corresponding to ceramic paper without active phases are also included. In these latter patterns (LF and SF), signals corresponding to the tetragonal zirconia, whose main peak is at 2θ = 30.2°, can be appreciated and correspond to the crystallized binder agent that coats and joins the silica-alumina fibers. Besides, the diffractogram of the short fiber-containing paper (SF) shows the main signals of the monoclinic ZrO_2 displayed at 28.2° and 31.5°, associated with ZrO_2 fibers.

Peaks located at 37.3; 43.3; 62.9; 75.5 and 79.6° associated with the presence of nickel oxide (NiO) can be observed in all diffractograms of the catalytic paper. The most intense peaks of zirconia can also be appreciated and depending on whether the paper is manufactured with or without ZrO_2 fibers, signals of monoclinic ZrO_2 are detected.

The crystalline domain sizes of nickel oxide were estimated at 9.7 nm for Ni (0.3 M) LF; 3.9 nm for NiZr 0.11 (0.3 M) LF; 3.6 nm for NiZr 0.15 (0.3 M) LF and 3.0 nm for NiZr 0.11 (0.3 M) SF. These results indicate that the presence of zirconium, incorporated as promoter, inhibits the development of the nickel oxide crystallites in all cases. Furthermore, the presence of short ZrO_2 fibers also seems to restrict the growth of NiO crystallites, which suggests some kind of Ni-Zr interaction.

The paper prepared with the 0.4 M precursor solution showed similar diffraction patterns to those described above (not shown). However, the sizes of the crystalline domains of NiO were higher in

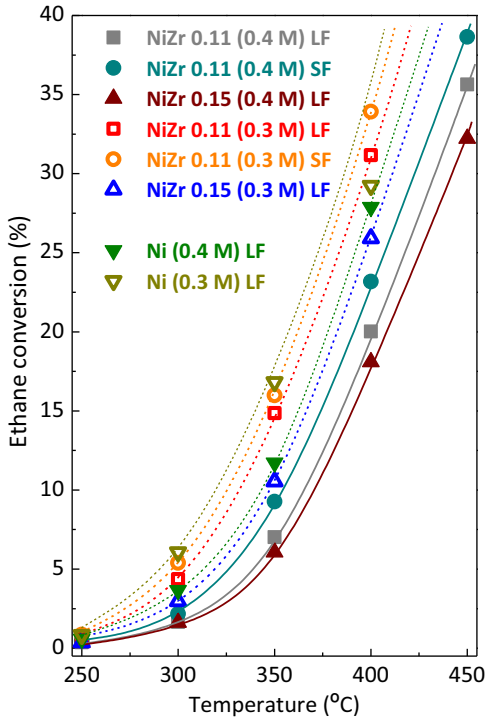

Fig. 6. Ethane conversion as a function of temperature for catalytic paper (T = variable, W/F = 0.48 g s/cm^3).

all cases. For this set of catalysts, they were estimated at 10.5 nm for Ni (0.4 M) LF and for the promoter-containing systems at 5.5 nm for NiZr 0.11 (0.4 M) LF; 5.2 nm for NiZr 0.15 (0.4 M) LF and 4.0 nm for NiZr 0.11 (0.4 M) SF, showing the same trend as the one observed in the above mentioned systems. Once more, the presence of the zirconia short fibers inhibited the crystalline growth of NiO.

The redox behavior of the catalytic components is an important property for the catalysts under study. Thus, temperature-programmed reduction experiments were carried out. Profiles obtained are presented in Fig. 4. A reduction peak between ~300 and 550 °C, associated with the reduction of nickel oxide is observed for Ni (0.3 M) LF. The reduction process begins at a temperature below 300 °C while the maximum is shown at ~420 °C. The pattern corresponding to Ni (0.4 M) LF appears ~10 °C left shifted, both at the onset and at the maximum temperatures if compared with Ni (0.3 M) LF TPR profile. This could be caused by a different degree of interaction between the catalytic particles and the zirconia coating of ceramic fibers, being it slightly stronger for Ni (0.3) M LF.

Zirconium-containing catalysts showed a marked broadening with a maximum at ~500 °C and a shift in reduction temperatures to higher values as compared with promoter-free catalysts. Therefore, the interaction between Ni and Y-Zr generated species more difficult to reduce, even in the case of smaller NiO crystallites. It is likely that Zr introduces itself into NiO lattice, forming a solid solution, which is probable since Ni^{2+} and Zr^{4+} cations have similar ionic radii. In this respect, as reported by Wu et al. [23], the incorporation of zirconium in the nickel oxide lattice retarded the reduction process. On the contrary, the incorporation of nickel ion into the zirconia lattice is more difficult due to its lower valence and its low solubility into the zirconia phase [24,25].

The main peak and the shoulder in Zr-promoted catalysts clearly indicate the reduction of different nickel species. The shoulder at lower temperatures – between 340 and 395 °C – is associated with the reduction of NiO, whereas the main peak could be ascribed to Ni-O-Zr species [23,26]. The increase in the zirconium content from Zr/Ni = 0.11 to Zr/Ni = 0.15 shifted the TPR profile toward higher temperatures. Also, it can be observed that a lower area of the shoulder is in agreement with the incorporation of Zr into the NiO lattice.

On the other hand, the addition of zirconia short fibers (SF) also produced a decrease in the shoulder area compared with the corresponding long fibers (LF) system, probably because of a higher dispersion of the active phase that enhances the Ni-Zr interaction. What is more, these systems display a slight shift in the TPR profile towards lower temperatures that could be related to the smaller crystallite size of the active phases (Fig. 4).

It should also be emphasized that both bare ceramic paper free of active phases (LF and SF, only coated with the yttria-zirconia binder) did not show hydrogen consumption in the temperature range analyzed, indicating the absence of reducible species.

Fig. 5 presents Raman spectra of the systems prepared with the 0.3 M solution. Spectra corresponding to catalytic ceramic paper prepared using the 0.4 M solution were similar (not shown). As reported, nickel oxide exhibits a Raman band around 500 cm^{-1}, assigned to first order longitudinal optical (LO) phonon mode, and a shoulder at ~400 cm^{-1} related to the transverse optical (TO) phonon mode [27,28]. The first order TO and LO modes derive from parity-breaking defects and are related to Ni vacancies in the oxygen-rich NiO particles (black coloured).

In the case of tetragonal zirconia, it is expected to have bands at 148, 263, 325, 472, 608 and 640 cm^{-1} while the monoclinic phase displays their main signals located at 140, 173, 185, 216, 260, 301, 328, 342, 471, 500, 553 and 632 cm^{-1} [29–32].

Although several zones were analyzed for catalytic ceramic paper, the characteristics bands of zirconia were not identified in any of the spectra. This could be associated with the location of the examined regions, in which only the active phase and not the zirconium-yttrium oxide from binder agent was detected. It must be noted that there appear to come into view only those signals corresponding to TO and LO modes and which related to NiO particles deposited on ceramic fibers.

Spectra of NiZr paper showed similar bands as compared with the free-promoter catalyst. Nevertheless, a comparison between Ni and NiZr catalysts illustrates differences. To begin with, the band corresponding to Ni—O stretching is markedly broadened, which could indicate an increased structural disorder [33,34]. In addition, this main band was markedly shifted (from ca. 500 to ca. 520 cm^{-1}), which confirms the strong interaction between nickel and the Zr promoter detected from TPR profiles. Furthermore, the shift observed would not be related to a size-induced phonon confinement effect, which would also produce a red shift [33], but could be strongly connected to the presence of the promoter [35,36]. The partial replacement of a Ni site into the nickel oxide lattice by another element leads to a modification in the cell volume. Lattice contraction or expansion produces changes in the unit cell parameters that modify Raman frequencies.

The above observations suggest changes into the NiO structural arrangement, confirming that zirconium was incorporated into the nickel oxide lattice and was not segregated as ZrO_2. At the same time, the absence of the typical zirconia bands confirms this idea and it is consistent with XRD and TPR characterization.

3.2. Catalytic performance of structured systems

Regarding catalytic performance, it is necessary to mention that selective reaction is the dehydrogenation of ethane to produce ethylene and that by the oxidative environment, water is produced as a by-product. Moreover, other non-selective reactions occur that produce carbon oxides and water, i. e. reactant and/or product could be oxidized. The carbon oxides formed could be monoxide and/or dioxide, but it depends on operation conditions, such as the oxygen/alkane ratio, as well as the nature of the catalyst.

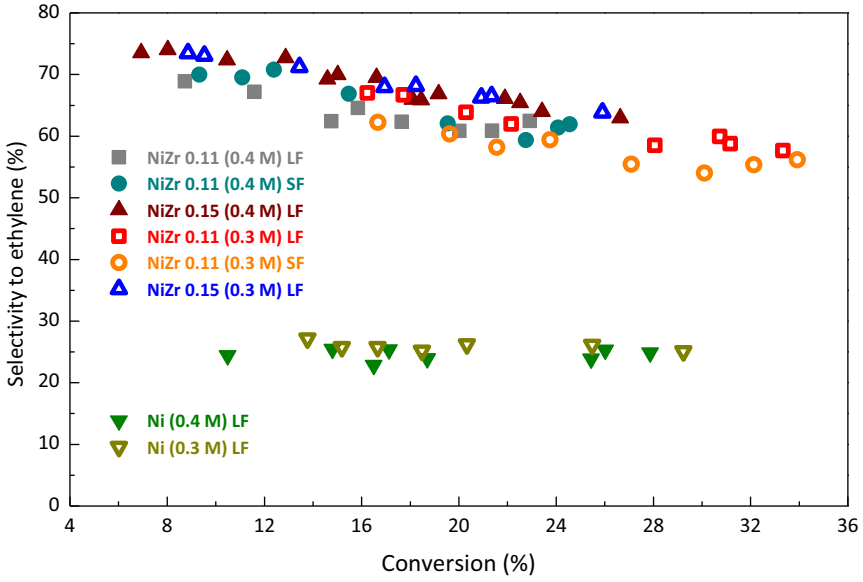

Fig. 7. Ethylene selectivity at constant temperature (T = 400 °C, W/F = variable).

To evaluate the catalytic behavior of the synthesized paper, the amount of oxygen used for the experiments was twice the stoichiometric, i.e. oxygen to alkane ratio equal to 1. This is one of the reasons that could contribute to the absence of CO as a product of non-selective reactions. This point could be considered as an advantage for future technological application, because the absence of carbon monoxide seems to be attractive not only for the simplification of subsequent separation processes but also for their safety.

In order to assess the effect of the zirconia binder on catalytic activity, several ceramic paper discs covered with yttria-stabilized zirconia were piled up into the reactor and they were evaluated showing only 0.6% ethane conversion at 450 °C.

Results of ethane conversion as a function of temperature of the catalytic ceramic papers are shown in Fig. 6. In general, the concentration of the precursor solution has an effect on the activity: those systems prepared with the 0.3 M solution are more active due to the smaller crystallites of the active phase and the better spreading onto the fibers, allowing better accessibility of the reagents to the catalyst surface.

In all cases, the addition of zirconium resulted in lower catalytic activities as compared with that of paper without a promoter (not shown). However, the effect depends on both the amount and the way zirconium is incorporated into the system through the $Zr(NO_3)_4$ solution or by means of adding ZrO_2 fibers. In the first case, a higher amount of promoter added to the precursor solution is negative for the ethane conversion since the presence of zirconium affects NiO reducibility. Also, it could reduce the amount of highly active oxygen species present in the non-selective bulk nickel oxide [6,7]. In the second case, the addition of ZrO_2 fibers to the structure could improve the dispersion of the active phases and help to achieve even smaller crystallite sizes compared with the paper that does not contain this kind of fibers. Besides, the reducibility of this system happened to be slightly higher as shown by TPR patterns. Therefore, the combination of all these factors contributes to increase the conversion.

Results of selectivity at constant temperature are presented in Fig. 7. The general trend for NiZr systems is a slight drop of around 10% in the conversion range analyzed. This slight decrease corresponds to the oxidation of the ethylene formed and it is indicative of the fact that carbon dioxide comes mainly from the direct oxidation of ethane and not from the oxidation of the main product.

It is necessary to mention that paper without a promoter showed very low selectivity to ethylene, with values in the order of 25%, which remained approximately constant with increasing conversion (not shown). The addition of zirconium resulted in a substantial improvement in the selectivity level. If the systems promoted are compared with one another, no substantial differences are observed, although the two kinds of paper with the higher amount of zirconium added to the precursor solution, i. e. Zr/Ni = 0.15, are more selective than the other ones. This could be partially explained by lower conversion as well as because of the fact that the promoter helps to reduce and isolate electrophilic oxygen species (O_2^-), which are more selective to carbon dioxide.

Table 1
Results reported in literature for different catalysts applied to ODH of ethane.

Catalyst [a]	W/F ratio (g s/cm^3)	Temperature (°C)	Ethane conversion (%)	Ethylene yield (%)	Reference
NiZr (0.3 M) SF [b]	0.48	400	34	19	This work
NiGaO	0.54	400	~31	~16	[2]
NiAlO	0.54	400	~25	~15	[2]
NiSnO	0.80	350	26	20	[24]
NiWO	0.60	400	~36	~23	[34]
$NiNbO/Al_2O_3$	0.54	400	27	~19	[9]
NiNbO	0.54	350	33	26	[10]
NiNbO	0.60	400	~56	~34	[37]
NiWO	–	400	~12	~5	[38]

[a] Powder catalyst.
[b] Structured catalyst.

Table 1 presents some results reported in the literature about Ni-containing powder catalysts applied to ODH of ethane reaction. It can be seen that the catalytic ceramic paper prepared presents promissory values of ethane conversion with moderate selectivity, even at high conversion levels (~60% selectivity at 34% of conversion). It is worth to mention that the W/F ratio employed in this work is the lowest among those listed in Table 1.

On the other hand, in order to assess the evolution of the conversion and selectivity over time, some catalysts prepared were tested under reaction conditions during 16 h. A slight decrease in ethane conversion was observed while a relative constancy on ethylene selectivity was found. These results give a first approach to the stability of this kind of structured systems under reaction conditions.

4. Conclusions

Catalytic ceramic paper could be successfully developed by the replacement of 10 wt% SiO_2-Al_2O_3 long fibers by ZrO_2 shorter ones.

Zirconium strongly interacted with nickel oxide and produced structural changes that affected the NiO redox behavior, crystal growth and lattice order (XRD, TPR, Raman), which enhanced selectivity towards ethylene.

Modifications introduced in the preparation process of NiZr-ceramic paper, i.e., the variation of the concentration of the precursor solution used and the addition of zirconia short fibers, allow obtaining systems with an enhanced performance.

Acknowledgements

The authors wish to acknowledge the financial support received from ANPCyT, CONICET, SECTEI Santa Fe and UNL.

References

[1] J.J.H.B. Sattler, J. Ruiz-Martinez, E. Santillan-Jimenez, B.M. Weckhuysen, Chem. Rev. 114 (2014) 10613–10653.
[2] E. Heracleous, A.A. Lemonidou, J. Catal. 270 (2010) 67–75.
[3] T. Chen, W. Li, C. Yu, R. Jin, H. Xu, Stud. Surf. Sci. Catal. 130 (2000) 1847–1852.
[4] Z. Skoufa, E. Heracleous, A.A. Lemonidou, Chem. Eng. Sci. 84 (2012) 48–56.
[5] L. Čapek, L. Vaněk, J. Adam, L. Smoláková, Stud. Surf. Sci. Catal. 174 (2008) 1175–1178.
[6] X. Zhang, J. Liu, Y. Jing, Y. Xie, Appl. Catal. A: Gen. 240 (2003) 143–150.
[7] K.I. Nakamura, T. Miyake, T. Konishi, T. Suzuki, J. Mol. Catal. A 260 (2006) 144–151.
[8] K. Sakitani, K. Nakamura, N. Ikenga, T. Miyake, T. Suzuki, J. Jpn. Petrol. Inst. 53 (2010) 327–335.
[9] E. Heracleous, A.F. Lee, K. Wilson, A.A. Lemonidou, J. Catal. 231 (2005) 159–171.
[10] E. Heracleous, A.A. Lemonidou, J. Catal. 237 (2006) 162–174.
[11] B. Solsona, P. Concepción, S. Hernández, B. Demicol, J.M. López Nieto, Catal. Today 180 (2012) 51–58.
[12] B. Solsona, P. Concepción, B. Demicol, S. Hernández, J.J. Delgado, J.J. Calvino, J.M. López Nieto, J. Catal. 295 (2012) 104–114.
[13] H. Zhu, D.C. Rosenfeld, D.H. Anjum, S.S. Sangaru, Y. Saih, S. Ould-Chikh, J.M. Basset, J. Catal. 329 (2015) 291–306.
[14] T.T. Nguyen, L. Burel, D.L. Nguyen, C. Pham-Huu, J.M.M. Millet, Appl. Catal. A: Gen. 433–434 (2012) 41–48.
[15] A. Löfberg, A. Essakhi, S. Paul, Y. Swesi, M.L. Zanota, V. Meille, I. Pitault, P. Supiot, B. Mutel, V. Le Courtois, E. Bordes-Richard, Chem. Eng. J. 176–177 (2011) 49–56.
[16] J.P. Bortolozzi, T. Weiss, L.B. Gutierrez, M.A. Ulla, Chem. Eng. J. 246 (2014) 343–352.
[17] J.P. Bortolozzi, L.B. Gutierrez, M.A. Ulla, Catal. Commun. 43 (2014) 197–201.
[18] J.P. Bortolozzi, E.D. Banús, D. Terzaghi, L.B. Gutierrez, V.G. Milt, M.A. Ulla, Catal. Today 216 (2013) 24–29.
[19] J.P. Bortolozzi, E.D. Banuís, V.G. Milt, E.E. Miro, Ind. Eng. Chem. Res. 53 (2014) 17570–17579.
[20] J.A. Santander, E. López, G.M. Tonetto, M.N. Pedernera, Ind. Eng. Chem. Res. 53 (2014) 11312–11319.
[21] B. Chu, L. Truter, T.A. Nijhuis, Y. Cheng, Catal. Sci. Technol. 5 (2015) 2807–2813.
[22] F.E. Tuler, E.D. Banús, M.A. Zanuttini, E.E. Miró, V.G. Milt, Chem. Eng. J. 246 (2014) 287–298.
[23] Y. Wu, J. Gao, Y. He, T. Wu, Appl. Surf. Sci. 258 (2012) 4922–4928.
[24] G. Štefanić, M. Didović, S. Musić, J. Mol. Struct. 834–836 (2007) 435–444.
[25] R.M. Batista, E.N.S. Muccillo, ECS Trans. 13 (2008) 47–54.
[26] K.K. Mohaideen, W. Kim, W.L. Yoon, Catal. Commun. 71 (2015) 7–12.
[27] W.J. Duan, S.H. Lu, Z.L. Wu, Y.S. Wang, J. Phys. Chem. C 116 (2012) 26043–26051.
[28] A.C. Gandhi, J. Pant, S. Pandit, S. Dalimbkar, T.S. Chan, C.L. Cheng, Y.R. Ma, S.Y. Wu, J. Phys. Chem. C 117 (2013) 18666–18674.
[29] B.K. Kim, H. Hamaguchi, Phys. Stat. Sol. 203 (1997) 557–563.
[30] T. Yamamoto, T. Tanaka, S. Takenaka, S. Yoshida, T. Onari, Y. Takahashi, T. Kosaka, S. Hasegawa, M. Kudo, J. Phys. Chem. B 103 (1999) 2385–2393.
[31] T.T. Ali, K. Narasimharao, N.S. Ahmed, S. Basahel, S. Al-Thabaiti, M. Mokhtar, Appl. Catal. A: Gen. 486 (2014) 19–31.
[32] T.M.C. Hoang, N.K. Rao, L. Lefferts, K. Seshan, ChemCatChem 7 (2015) 468–478.
[33] D.J. Kim, H.J. Jung, I.S. Yang, J. Am. Ceram. Soc. 76 (1993) 2106–2108.
[34] H. Zhu, H. Dong, P. Laveille, Y. Saih, V. Caps, J.M. Basset, Catal. Today 228 (2014) 58–64.
[35] F. Ahmed, N. Arshi, M.S. Anwar, S.H. Lee, E.S. Byon, N.J. Lyu, B.H. Koo, Curr. Appl. Phys. 12 (2012) S174–S177.
[36] S. Liu, J. Jia, J. Wang, S. Liu, X. Wang, H. Song, X. Hu, J. Magn. Magn. Mater. 324 (2012) 2070–2074.
[37] H. Zhu, D.C. Rosenfeld, D.H. Anjum, V. Caps, J.-M. Basset, ChemSusChem 8 (2015) 1254–1263.
[38] B. Solsona, J.M. López Nieto, P. Concepción, A. Dejoz, F. Ivars, M.I. Vázquez, J. Catal. 280 (2011) 28–39.